linear 2-fold to square planar. While the square-pyramidal coordination around the Cu(2) is maintained, there is an effect on the vertical bond length since the affected Cu(1) is directly coupled to Cu(2) by an oxygen atom. A contraction in c axis occurs, and the overall sample length shrinks.

When a correlation between Ca content x and expansion is sought, it is seen that the location of the Ca in the rare-earth metal plane is too distant to affect directly the O–Cu–O bonding which seems to cause the enormous expansivity changes. A kinetic explanation based on the weight changes previously observed for various Ca contents[3] is suggested. The earlier work showed that for a slower heating rate (1 °C/min) all Ca contents (x = 0.0, 0.25, and 0.40) gained similar amounts while faster rates (2 and 5 °C/min) produce lower weight gains for x = 0.0. In this study the dilatometric data were obtained at 4 °C/min for all Ca contents. Thus the x = 0.0 expansion represents material that has not achieved full oxidation. When Ca is present, more expansion is obtained at the same heating rate. It is therefore suggested that Ca has the effect of facilitating the oxidation process so that oxygen can more quickly enter the lattice and more expansion occurs at the heating rate used.

Conclusions

Oxidation and reduction of $Pb_2Sr_2Y_{1-x}Ca_xCu_3O_{8+\delta}$ produce very large changes ($\sim 5 \times 10^{-3}$) in the dimensions of ceramic samples.

Within the orthorhombic/tetragonal phase region these changes are the result of changes in lattice dimensions, particularly the c parameter.

At 550 °C the oxidation of $Pb_2Sr_2YCu_3O_8$ is much slower than reduction.

The decomposition of the orthorhombic/tetragonal phase to pseudocubic produces an enlarged structure.

The Ca content affects the rate of the oxidative expansion with increasing x producing faster oxidation and more expansion at 350–600 °C for a constant heating rate.

Changes in oxygen content produce opposite expansions in $Ba_2YCu_3O_7$ and $Pb_2Sr_2YCu_3O_8$.

Acknowledgment. We are grateful to R. J. Cava for helpful discussions.

Registry No. $Pb_2Sr_2Y_{0.8}Ca_{0.2}Cu_3O_8$, 122408-19-9; $Pb_2Sr_2Y_{0.6}Ca_{0.4}Cu_3O_8$, 122408-20-2; $Pb_2Sr_2YCu_3O_8$, 118557-29-2.

Particle Size Determination of Cobalt Clusters in Zeolites

Sang Sung Nam,[†] Lennox E. Iton,[‡] Steven L. Suib,*[,†,§] and Z. Zhang[†]

Department of Chemistry, U-60, University of Connecticut, Storrs, Connecticut 06269-3060, Materials Science Division, Argonne National Lab, Argonne, Illinois 60439, and Department of Chemical Engineering, University of Connecticut, Storrs, Connecticut 06269-3060

Received June 5, 1989

Highly dispersed superparamagnetic cobalt clusters have been prepared in the pores of zeolite Na–X by use of microwave plasma decomposition of $Co_2(CO)_8$. These cobalt clusters have previously been shown to be 100% dispersed and are shown here to be stable to 160 °C. Ferromagnetic resonance data have been simulated to show that the cobalt clusters have a 7-Å-diameter size. Transmission electron microscopy experiments have shown that the cobalt particles are not observable unless sintering at 160 °C occurs. These results are correlated to the catalytic activity of the cobalt clusters in reactions of cyclopropane and hydrogen. The size of the cobalt clusters controls the selectivity of these catalytic reactions.

Introduction

One of the goals of researchers in the area of catalysis in the past 10 years has been the preparation of highly dispersed materials such as metal clusters.[1] Several approaches have been taken, including solvated metal atom dispersion (SMAD),[2] cluster-derived thermal decompositions,[3] metal atom vaporization,[4] metal vapor reduction,[5] H atom reduction,[6] anchoring,[7] ion implantation,[8] and other methods. When a solid is used to trap the metal clusters, it may be possible to prepare particles smaller than about 15 Å. In this size regime such metal particles may not behave like bulk metals and can give rise to interesting new physical and chemical properties.[9]

Heterogeneous catalytic reactions that depend on the size and shape of metal particles are said to have geometric effects. Electronic effects are due to bonding interactions between the metal and its support.[10] Electronic effects can be difficult to measure, and there has been consider-

[†] Department of Chemistry.
[‡] Materials Science Division.
[§] Department of Chemical Engineering.
* Author to whom correspondence should be addressed at the Department of Chemistry, University of Connecticut.

(1) Moskovits, M., Ed. *Metal Clusters*; Wiley Interscience: New York, 1986.
(2) (a) Klabunde, K. J.; Imizu, Y. *J. Am. Chem. Soc.* **1984**, *106*, 2721–2722. (b) Tan, B. J.; Klabunde, K. J; Tanaka, T.; Kanai, H.; Yoshida, S. *J. Am. Chem. Soc.* **1988**, *110*, 5951–5958. (c) Meier, P. F.; Pennella, F.; Klabunde, K. J. *J. Catal.* **1986**, *101*, 545–548.
(3) (a) Uchiyama, S.; Gates, B. C. *J. Catal.* **1988**, *110*, 388–403. (b) Gates, B. C. In *Catalyst Design, Progress and Perspectives*; Wiley Interscience: New York, 1987; pp 71–139.
(4) (a) Klabunde, K. J. *Chemistry of Free Atoms and Particles*; Academic Press: New York, 1980. (b) Nazar, L. F.; Ozin, G. A.; Hugues, F.; Godber, J.; Rancourt, D. *Angew. Chem., Int. Ed. Engl.* **1983**, *22*, 624–625.
(5) (a) Fraenkel, D.; Gates, B. C. *J. Am. Chem. Soc.* **1980**, *102*, 2478–2480. (b) Lee, J. B. *J. Catal.* **1981**, 68, 27–33.
(6) Bonneviot, L.; Che, M.; Olivier, D.; Martin, G. A.; Freund, E. *J. Phys. Chem.* **1985**, *90*, 2112–2117.
(7) (a) Jiang, H. J.; Tzou, M. S.; Sachtler, W. M. H. *Appl. Catal.* **1988**, *39*, 255–265. (b) Tzou, M. S.; Teo, B. K.; Sachtler, W. M. H. *Langmuir* **1986**, *2*, 773–776. (c) Tzou, M. S.; Teo, B. K.; Sachtler, W. M. H. *J. Catal.* **1988**, *113*, 220–235.
(8) Haining, I. H. B.; Rabette, P.; Che, M.; Deane, A. M.; Tench, A. J. *Proc. Int. Congr. Catal., 7th* **1980**, 317–322.
(9) Romanowski, W. *Highly Dispersed Metals*; Halsted Press: New York, 1987.

0897-4756/89/2801-0529$01.50/0

able debate about such phenomena. In fact, it is often difficult to separate geometric and electronic effects since they may operate in tandem. If geometric or electronic effects influence a catalytic reaction, these are called structure-sensitive (or demanding) reactions.[11] Once the roles of geometric or electronic effects are understood, it may be possible to prepare more active and selective catalytic materials.

Metal-containing zeolites have been studied for quite some time, and this is the subject of a recent review.[12] Cobalt clusters have been prepared in zeolites by Cd vapor[3a] and metal atom vaporization methods.[4b] The key in many cases has been to avoid the ionized state (i.e., ion exchange) since it is difficult to reduce all of the ions.

Our approach has been to incorporate zerovalent organometallic precursors such as $Co_2(CO)_8$ into dehydrated zeolites followed by decomposition in a microwave plasma.[13] These CoNa–X materials as well as those prepared by metal atom vaporization methods[4b] show unusually high selectivity toward olefins in Fischer–Tropsch catalysis.[14] Our materials have been characterized by several spectroscopic methods such as ferromagnetic resonance,[13] chemisorption,[15] spin echo nuclear magnetic resonance,[16] transmission electron microscopy,[17] and other methods to determine the size and shapes of the cobalt particles, their oxidation states, and the particle size distribution.

In this paper we report the use of simulations of ferromagnetic resonance spectra to determine particle size, Rutherford backscattering to determine the relative surface and bulk Co concentrations, and transmission electron microscopy to study sintering and how these properties are related to catalytic activity.

Experimental Section

Sample Preparation. Zeolite Na–X was obtained from Alfa Ventron Co., Danvers, MA, and dehydrated at 375 °C at 1×10^{-5} Torr for 8 h. The dehydrated zeolite was loaded in a drybox into one well of a quartz reactor, and $Co_2(CO)_8$ was loaded into the other side of the reactor. The ends of the reactor were sealed off with shutoff valves, and the reactor was then connected to a vacuum line. Metal carbonyl was sublimed at room temperature onto the zeolite and decomposed in an Ar microwave plasma so as to produce a 0.8 wt % Co sample. The reactor was then evacuated, sealed off, and brought back into the drybox prior to catalytic, spectroscopic, and microscopic experiments. Further details of this general procedure can be found elsewhere.[13]

Ferromagnetic Resonance. About 0.2 g of the decomposed cobalt carbonyl in Na–X zeolite (CoNa–X) was loaded into a 2-mm-o.d. quartz tube and sealed off on a vacuum line prior to ferromagnetic resonance (FMR) experiments. FMR experiments were done on a Varian electron paramagnetic resonance E-3 spectrometer at temperatures between 133 and 333 K. Low-temperature experiments were done sequentially before raising the temperature to the next highest temperature to prevent adsorption of water in the cavity and to avoid sintering of the cobalt.

Simulations of the FMR data were done on an IBM XT computer. Details of the simulations will be described in the Discussion.

Transmission Electron Microscopy. Transmission electron microscopy (TEM) experiments were done at the Electron Microscopy Center at Argonne National Labs. Samples were prepared by microtoming CoNa–X samples embedded in a polymer matrix. A JEOL 100 CX transmission electron microscope was used for all TEM experiments.[17]

Rutherford Backscattering. Rutherford backscattering (RBS) experiments were done in CoNa–X zeolite samples with a General Ionex Tandetron spectrometer. A 2.2-MeV He^{2+} ion beam was used for backscattering. Two detectors were used to observe particles either normal or at grazing angles to the surface. Samples were spread on 1-in. carbon disks for this analysis. Theoretical depth profiles were generated by using procedures given elsewhere.[18]

Catalysis Experiments. Reactions of cyclopropane and hydrogen were carried out over CoNa–X zeolite in a flow reactor at temperatures from 100 to 200 °C. A 10/1 H_2/cyclopropane feed at 1 atm of total pressure was used. Samples were loaded into a stainless steel reactor of 12-in. length and 6-mm o.d. The temperature of the catalyst was monitored in the catalyst bed with a digital thermometer, and an Omega temperature controller was used for regulation of the temperature of the sample. Products were analyzed with a Hewlett-Packard Model 5880 A gas chromatograph equipped with a thermal conductivity detector and with Poropack Q columns. Details of the analytical procedures used are given elsewhere.[17]

Results

Ferromagnetic Resonance. Ferromagnetic resonance data for CoNa–X at room temperature are given in Figure 1a. Experimental data were digitized, and the theoretical fit was done with a procedure outlined below. In EPR and FMR, the position of the resonance lines observed is determined by the relationship $h\nu = gBHS$, where h is Planck's constant, ν is the frequency, g is an effective g value which for a free electron has the value 2.0023, B is the electron Bohr magneton, H is the applied field strength, and S is the spin operator. At −60 °C a new peak appeared at about $g = 4.3$ with an H value of about 1.6 kOe as shown in Figure 1b. This extra peak was fit with a second term in the Hamiltonian as described below. At −160 °C the peak at $g = 4.3$ grows in intensity with respect to the broad transition near $g = 2.0$ ($H = 2.9$ kOe) as shown in Figure 1c.

The apparent g value as obtained from the theoretical simulation decreases exponentially as a function of temperature as shown in Figure 2. The line width of the $g = 2.0$ signal decreases linearly as a function of increasing temperature as shown in Figure 3. These values were obtained from line-shape simulations.

Transmission Electron Microscopy. Transmission electron microscopy experiments were carried out on the CoNa–X zeolite material before catalytic reaction and after catalytic reactions at elevated temperature. TEM experiments showed no evidence of metal particles at the surface of the zeolite for all untreated CoNa–X zeolite samples prior to catalysis and for those catalysts treated at temperatures below 160 °C. Figure 4 shows a TEM photograph of CoNa–X prior to any catalytic testing of the material. This material had been decomposed in an Ar microwave plasma.

Samples of CoNa–X treated at temperatures above 160 °C prior to or during reactions with cyclopropane and

(10) (a) Takasu, Y.; Akimura, T.; Kasahara, K.; Matsuda, Y. *J. Am. Chem. Soc.* **1982**, *104*, 5249–5250. (b) Vedrine, J. C.; Dufaux, M.; Naccache, C.; Imelik, B., *J. Chem. Soc., Trans Faraday Soc. 1*, **1978**, *74*, 440–449. (c) Hendrickx, H. A. C. M.; Des Bouvrie, C. Ponec, V. *J. Catal.* **1988**, *109*, 120–125.

(11) (a) Boudart, M.; McDonald, M. A. *J. Phys. Chem.* **1984**, *88*, 2185–2195. (b) Carberry, J. J. *J. Catal.* **1988**, *114*, 277–283.

(12) Nicolaides, C. P.; Scurrell, M. S. In Keynotes in Energy Related Catalysis. Kaliaguine, S., Ed.; *Studies in Surface Science and Catalysis*; Elsevier: New York, 1988 Vol. 35, Chapter 6, pp 319–379.

(13) Zerger, R. P.; McMahon, K. C.; Seltzer, M. D.; Michel, R. G.; Suib, S. L. *J. Catal.* **1986**, *99*, 498–505.

(14) Suib, S. L.; McMahon, K. C.; Tau, L. M.; Bennett, C. O. *J. Catal.* **1984**, *89*, 20–34.

(15) McMahon, K. C.; Suib, S. L.; Johnson, B. G.; Bartholomew, C. H. *J. Catal.* **1987**, *106*, 47–53.

(16) Zhang, Z.; Suib, S. L.; Zhang, Y. D.; Hines, W. A.; Budnick, J. I. *J. Am. Chem. Soc.* **1988**, *110*, 5569–5571.

(17) Zhang, Z.; Suib, S. L. In *Perspectives in Molecular Sieves*; Flank, W. H., Whyte, T. E., Eds.; ACS Symposium Series: American Chemical Society: Washington, DC, 1988; No. 368, pp 569–578.

(18) (a) Baumann, S.; Strathman, M. D.; Suib, S. L. *J. Chem. Soc., Chem. Commun.* **1986**, 308–309. (b) Baumann, S.; Strathman, M. D.; Suib, S. L. *Anal. Chem.* **1988**, *60*, 1046–1051.

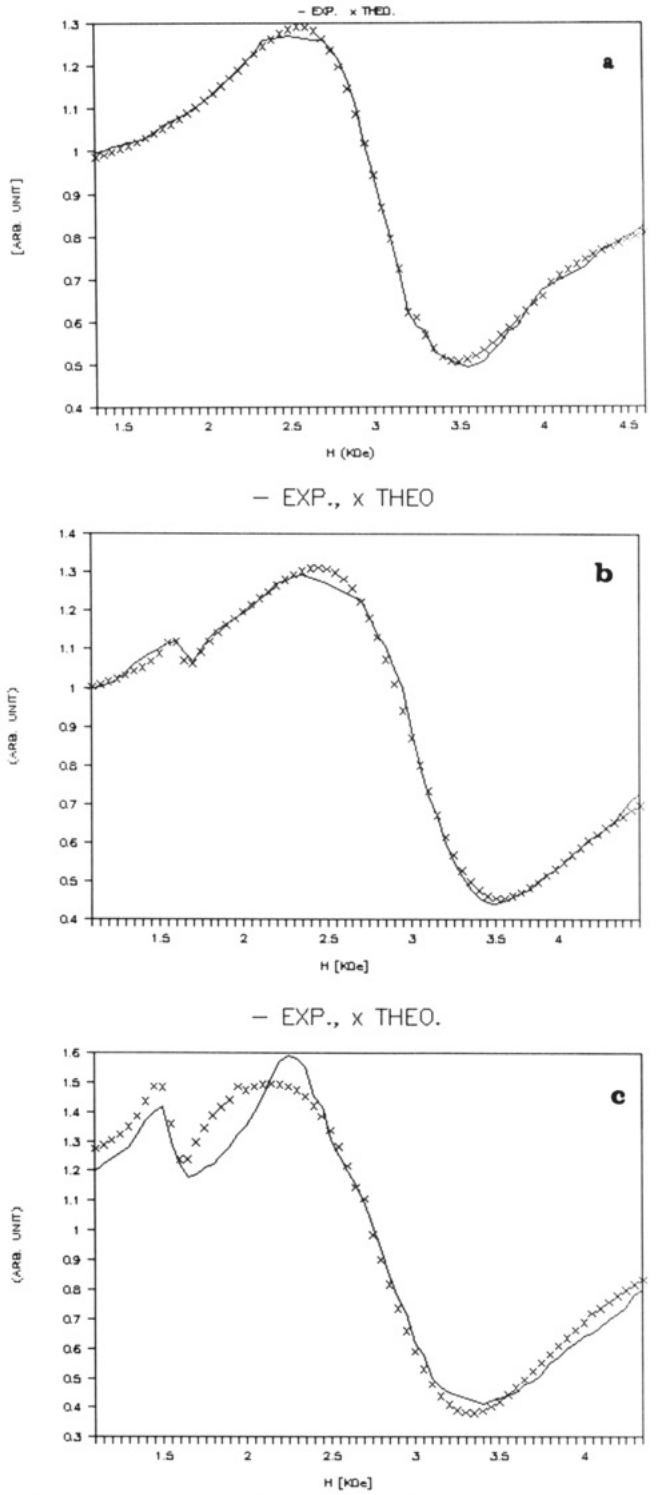

Figure 1. Ferromagnetic resonance data for CoNa–X zeolite at (a) room temperature, (b) –60 °C, and (c) –160 °C.

hydrogen show surfaces such as that of Figure 5. The darker spots and the mottled appearance show electron diffraction patterns consistent with those of bulk cobalt particles. Particle size distributions are between 15 and 20 Å.

Rutherford Backscattering. Rutherford backscattering data for CoNa–X are given in Figure 6. Figure 6A represents the raw RBS data for CoNa–X, while Figure 6B represents a theoretical fit of these data. Backscattering of oxygen is observed around channel number 180, sodium near channel number 260, Si and Al near channel number 300, and cobalt near channel number 400.

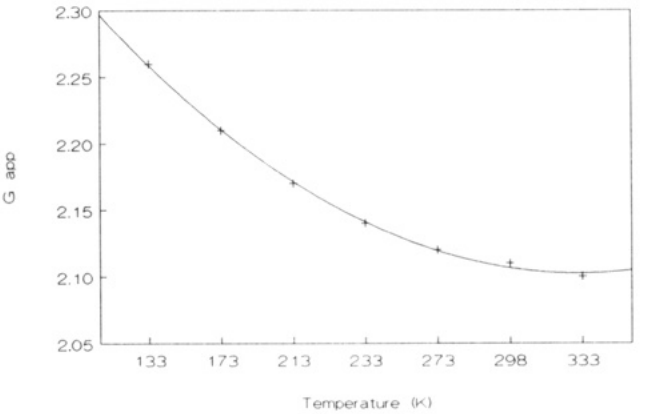

Figure 2. Ferromagnetic resonance data for CoNa–X: plot of simulated apparent g value as a function of temperature.

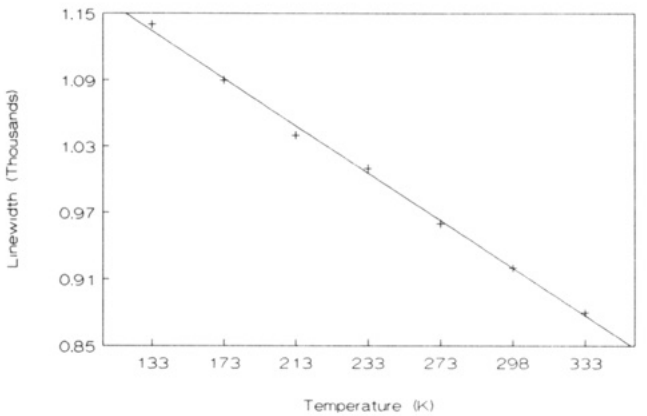

Figure 3. Ferromagnetic resonance data for CoNa–X: plot of simulated line width as a function of temperature.

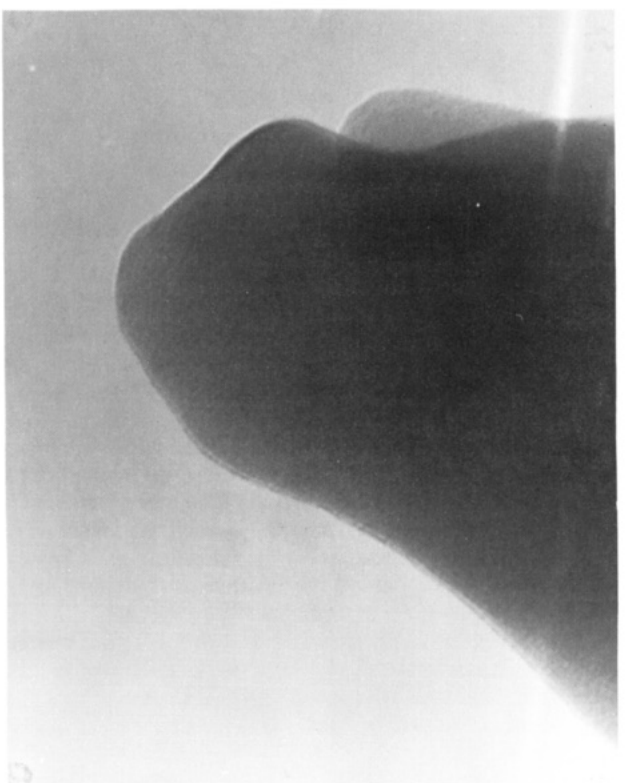

Figure 4. Transmission electron micrograph of CoNa–X, 137600× magnification.

A theoretical depth profile for CoNa–X based on the data of Figure 6 is given in Figure 7. The relative atomic fractions of Na, Si, and Al are slightly increasing as a function of depth into the sample, whereas the cobalt and

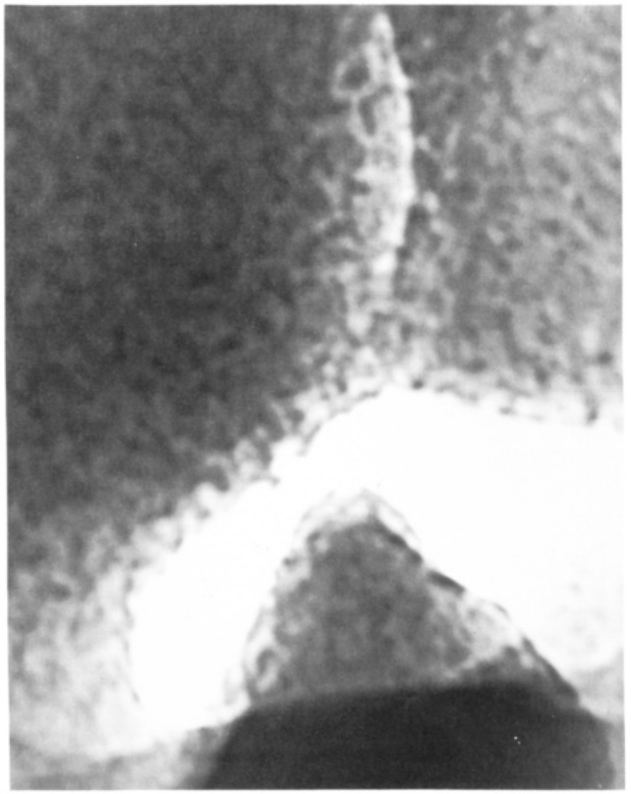

Figure 5. Transmission electron micrograph of CoNa–X after reaction with cyclopropane and hydrogen at 160 °C, 137600× magnification.

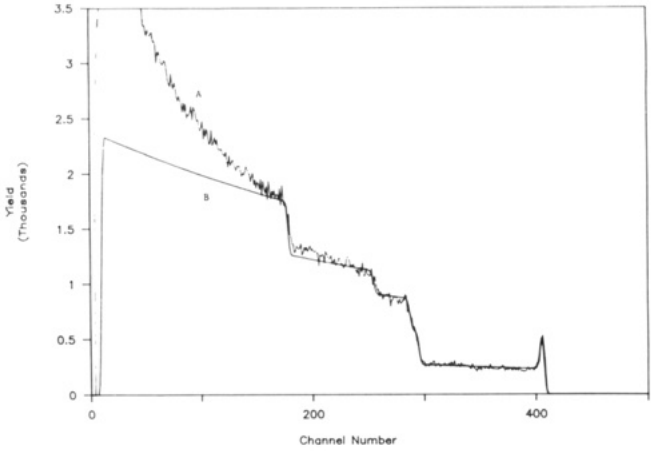

Figure 6. Rutherford backscattering data for CoNa–X: (a) experimental data; (b) theoretical fit.

oxygen atomic fractions markedly increase in the bulk of the material. A detailed description of the theory of RBS and these theoretical depth profiles is given elsewhere.[18]

Catalytic Experiments. Catalytic data for CoNa–X are summarized in Table I. For samples treated near 120 °C the only product observed was propylene. For temperatures of 160 °C the primary product was propane. At 200 °C propane, methane and ethane were detected. The ratio of methane to ethane was 1 at all times. These data were collected at steady state, after about 2 h on stream.

Discussion

Ferromagnetic Resonance. The $g = 4.3$ signal is due to an Fe^{3+} impurity in the framework of the zeolite which is in a rhombic crystal field.[19,20] A complete description

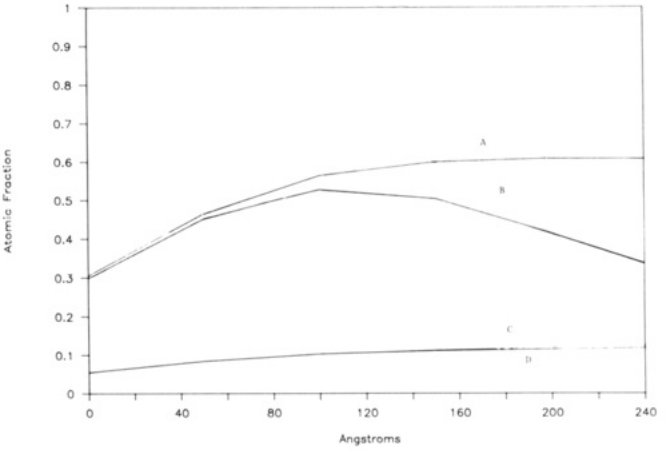

Figure 7. Rutherford backscattering theoretical depth profile: (a) oxygen; (b) cobalt; (c) silicon and aluminum; (d) sodium.

Table I. Catalytic Data for CoNa–X

temp, °C	turnover frequency[a]	product
120	0.9	propylene
160	1.5	propane
200	1.7	propane
	0.4	methane
	0.4	ethane

[a] $\times 10^4$, in mmol product per minute per gram of Co (0.8 wt % as determined by atomic absorption), 120 min of time.

of this species is beyond the scope of this paper; however, a spin Hamiltonian of the type

$$H = g_0 BHS + \tfrac{1}{3}(b_2^{\circ} O_2^{\circ} + b_2^2 O_2^2) \qquad (1)$$

can be used to describe this Fe^{3+} species. The first term is the Zeeman term, and the second term is a crystal-field term with second degree spin operators. In this Hamiltonian, H is the value of the magnetic field, B is the Bohr magneton, g_0 is the isotropic g value for Fe^{3+}, and B is the electron spin angular momentum term. Details concerning the crystal field terms can be found elsewhere[21] and have been used by us to describe the Eu^{2+} environment in zeolite A.[22]

The second broad transition centered around $g = 2.0$ was simulated using the method of Sharma and Baiker[23] for superparamagnetic particles. A Lorentzian line shape was assumed in this analysis, and the first derivative of the absorption curve was calculated with the following function:

$$y(H) = \sum_{\theta=0}^{\pi} \sum_{\phi=0}^{2\pi} k[H - H(\theta,O)]W(\sin\theta)/\{3W^2 + [H - H(\theta,O)]^2\}^2 \qquad (2)$$

where H is the value of the applied magnetic field, k is a normalization constant, y is the amplitude of the signal, W is the peak-to-peak line width of the derivative Lorentzian function, and θ and ϕ represent the angular dependence of the resonance field for an isotropic particle.

Our overall Hamiltonian, then, is a combination of eq 1 and 2. Notice that this Hamiltonian provides an excellent fit to the experimental data at room temperature and at −60 °C for Figure 1, parts a and b. On the other

(19) Iton, L. E.; Beal, R. B.; Hodul, D. T. *J. Mol. Catal.* **1983**, *21*, 151–171.
(20) Schmidt, F.; Meeder, T. *Surf. Sci.* **1981**, *106*, 397–402.
(21) Aasa, R. *J. Chem. Phys.* **1970**, *52*, 3919–3926.
(22) Iton, L. E.; Brodbeck, C. M.; Suib, S. L.; Stucky, G. D. *J. Chem. Phys.* **1983**, *79*, 1185–1196.
(23) Sharma, V. K.; Baiker, A. *J. Chem. Phys.* **1981**, *75*, 5596–5601.

hand, the agreement of the theoretical simulation and experimental data at −160 °C is not outstanding. The reason for this discrepancy is that at the −160 °C the particles are no longer superparamagnetic, and as a consequence there are extra anisotropic terms related to the shape of the particles and other factors that need to be included but at present are not available.

The agreement between experimental and theoretical data for the higher temperatures is quite good and in fact better than that of Sharma and Baiker.[23] However, a direct comparison between our data and theirs[23] is probably not wise since their data are for Ni and ours for Co and quite different matrices were used. We are not aware of other simulations of Co systems.

Values of line widths and apparent g factors for the broad transition near $g = 2.0$ can be obtained from the simulations, and these data are graphed in Figures 2 and 3. The apparent g value decreases as the temperature is increased, as expected for superparamagnetic Ni particles[24] and for Co particles[25] as shown in Figure 2. An asymptotic value for g_{app} can be obtained that is significantly lower than the $g = 2.18$ value for hexagonal closest packed Co particles and is more consistent with the $g = 2.06$ value reported for face-centered-cubic Co particles. In fact, spin echo nuclear magnetic resonance data for our CoNa–X sample indicate that these particles are face-centered cubic.[16]

The lower the temperature at which the $g = 2.06$ value is reached, the smaller the particle size.[22-25] For samples heated above 433 K the g values are larger at all temperatures, indicating that these Co particles sinter at temperatures at and above 433 K.[13,15] This conclusion is further supported by TEM data given below.

From the simulation it is possible to obtain values of the ansiotropic field (H_a) as well as normalization constant values (k_a) to determine the saturation magnetization, M_s as shown in eq 3. This is important since the volume of

$$H_a = k_a/M_s \quad (3)$$

the particles and hence the relative particle size can be obtained[26] from M_s by equation 4, where V is the particle

$$x = M_s VH/kT \quad (4)$$

volume and x is related through the Langevin (L) function:[27]

$$L(x) = \coth x - 1/x \quad (5)$$

for superparamagnetic particles whose direction of magnetization fluctuates at rates faster than the Larmor frequency, resulting in narrower resonance lines at high temperature due to averaging effects of such fluctuations on the magnetic anisotropy:

$$H_a^{sp} = H_a\{1 - 10x^{-1}L(x) + 35x^{-2} - 105x^{-3}L(x)\}/L(x) \quad (6)$$

where sp stands for superparamagnetic.

From eq 4–6 and the simulation values of M_s and with the assumption that particles are homogeneous and of the face-centered-cubic type,[16] we obtain a particle size of 7 Å. This is in good agreement with the 5-Å value determined by spin echo nuclear magnetic resonance methods[16] and chemisorption measurements.[15]

Several precautions should be mentioned about these simulations as well as the approach used to determine the particle size of the cobalt clusters. First, it should be realized that the Fe^{3+} rhombic field term was used as an internal standard for calibration of the magnetic field and the second term of the Hamiltonian of eq 1 was not rigorously solved as has been done previously.[21] Second, the use of eq 3–6 for the determination of Co particle size involves many assumptions[26,27] such as the uniform size of such clusters. Results from FMR, spin echo NMR, chemisorption, TEM (vide infra), and other methods suggest that there is a narrow distribution in particle size. The absence of large particles has led us to use the approximation that the particles are about the same size.

Transmission Electron Microscopy. TEM data shown in Figure 4 show that no cobalt particles are observed at the surface. Cobalt particles smaller than about 15 Å have not been observed for supported metal catalysts due to similarities in contrast between the metal and the support.[28] After heat treatment of the CoNa–X zeolite to 160 °C either before or after catalytic experiments, Co particles of 15-Å size are observed giving a mottled appearance. A reviewer has suggested that this may be due to aggregation of the cobalt in supercages which causes concomitant local damage to the zeolite.[31] These TEM data suggest that the small 5–7-Å particles residing in the pores of Na–X zeolite start to sinter around 160 °C. The Co particles may come out of the supercage pores during this sintering; however, no clear observation of metallic particles at the edges of the zeolite crystallites is apparent.

No attempt was made to look at the Si/Al ratio after heating to 160 °C, which should increase if local damage to the zeolite is occurring.[32] Adsorption isotherm data might also show that mesopores of the diameter of the metal particles are observed.[32] Such local damage and increased pore size might explain why the turnover frequencies increase after sintering due to greater accessibility of the reactants to the metal sites.

Rutherford Backscattering. The Rutherford backscattering data of Figure 6 show good agreement between experimental and theoretical fits for O, Na, Si, Al, and Co in CoNa–X. The theoretical depth profile of Figure 7 for CoNa–X prior to heat treatment is in line with the suggestion that most of the Co resides in the pores of the zeolite. Similar RBS experiments have been done for a variety of rare-earth metal and actinide zeolites, and it is possible to establish whether metals reside solely on the surface of the zeolite or whether some metal ions (and in this case metal particles) reside inside zeolite pores.[18] Microscopy[31] and Xe NMR experiments[32] are also useful in this regard. Data reported here are consistent with our belief that adsorption of $Co_2(CO)_8$ (which has dimensions of about 5.2 × 5.3 Å) into the pores of zeolite Na–X followed by decomposition in an Ar plasma leads to highly dispersed Co particles in the pores of the zeolite. In fact, we have not been able to prepare such highly dispersed particles in nonmolecular sieve supports.[13]

Catalysis Data. The catalysis data of Table I serve to summarize the overall reactivity of the highly dispersed Co clusters in Na–X zeolite with cyclopropane and hydrogen mixtures. At low temperature the only observed product is propylene. This comes about via ring-opening

(24) (a) Che, M.; Richard, M.; Olivier, D. *J. Chem. Soc., Faraday Trans.* **1980**, *76*, 1526–1534. (b) Derouane, E. G.; Simoens, A.; Colin, C.; Martin, G. A.; Dalmon, J. A.; Vedrine, J. C. *J. Catal.* **1978**, *52*, 50–58.
(25) Kim, J. C.; Woo, S. I. *Appl. Catal.* **1988**, *39*, 107–121.
(26) de Biasi, R. S.; Devezas, T. C. *J. Appl. Phys.* **1978**, *49*, 2466–2473.
(27) Sharma, V. K.; Waldner, F. *J. Appl. Phys.* **1977**, *48*, 4298–4303.
(28) (a) Fu, L.; Bartholomew, C. H. *J. Catal.* **1985**, *92*, 376–387. (b) Jones, R. D.; Bartholomew, C. H. *Appl. Catal.* **1988**, *39*, 77–88.
(29) Efstathiou, A.; Suib, S. L.; Bennett, C. O. Submitted to *J. Catal.*
(30) Imizu, Y.; Klabunde, K. J. In *Catalysis of Organic Reactions*; Augustine, R. L., Ed.; Marcel-Dekker: New York, 1985; pp 225–250.
(31) Gallezot, P.; Mutin, I.; Dalmai-Imelik, G.; Imalik, B. *J. Microsc. Spectrosc. Electron.* **1976**, *1*, 1–6.
(32) Jaeger, N. I.; Rathovsky, J.; Sculz-Ekloff, G.; Svensson, A.; Zukal, A. In *Zeolites, Facts, Figures, Future*; Jacobs, P. A., Van Santen, R. A., Eds.; Elsevier: Amsterdam, 1989; pp 1005–1013.

reactions such as

$$-C_3H_6 \xrightarrow{H_2} C_3H_6 \quad (7)$$

At 160 °C hydrogenation of the cyclopropane (c-C_3H_6) to propane occurs according to the following reaction:

$$c\text{-}C_3H_6 + H_2 \rightarrow C_3H_8 \quad (8)$$

At even higher temperatures near 200 °C hydrogenolysis reactions occur leading to the formation of methane and ethane:

$$c\text{-}C_3H_6 + 2H_2 \rightarrow CH_4 + C_2H_6 \quad (9)$$

Since the ratio of methane to ethane is always 1 and since these CoNa–X catalysts are inactive toward cracking of propylene or propane to methane and ethane, then the formation of methane and ethane observed in our reactions is due to primary cracking of cyclopropane.

These catalysts are relatively unreactive with cyclopropane as compared to Co prepared by SMAD techniques.[30] This may be due to differences in preparation methods, different metal particle sizes, type of support, and type of adsorption site. The accessibility of reactant to metal sites may also be an important difference between these two types of materials. In fact, we have recently shown that molecular H_2 is trapped in sodalite cages of the zeolite[29] and that there is an activation barrier to overcome to obtain adjacent sites for both H and cyclopropane adsorption prior to reaction.

Overview. The FMR, TEM, RBS, and other spectroscopic data reported elsewhere[13-18] suggest that superparamagnetic Co particles are formed in the pores of Na–X and are of the order of 5–7 Å in size prior to thermal and catalytic treatment. If the temperature is raised above 160 °C, then the Co clusters begin to aggregate and sinter perhaps in the supercages of the zeolite. The temperature dependence of the selectivity of cyclopropane and hydrogen over these Co clusters suggests that the smaller Co clusters do not appreciably dissociate H_2, whereas intermediate size clusters produced at 160 °C allow dissociation of H_2 and enough room for two adsorbed H atoms with cyclopropane. For the highest temperature, there is now room on the largest particle sizes for adsorption of four hydrogens as well as cyclopropane. These data suggest a structure sensitivity for the reaction of cyclopropane and hydrogen over CoNa–X.

Chemisorption data for the CoNa–X zeolite have been reported previously[15] and suggest that the Co clusters are essentially 100% dispersed. Such data have been reproduced in several labs for similarly prepared materials with consistent results.[15,29] Further studies using chemisorption indicate that the H chemisorption in these systems is not due to H spillover and that the H chemisorption process is activated. Molecular H_2 is initially trapped in sodalite cages as determined by transient studies. These factors suggest that it will be difficult to use H chemisorption for particle size determinations in CoNa–X and related systems. Results of these chemisorption and temperature-programmed desorption experiments will be presented elsewhere.[29]

Conclusion

Results of our ferromagnetic resonance simulations show that Fe^{3+} impurities as well as Co superparamagnetic particles are present in CoNa–X. FMR simulations also lead to particle size determination. The TEM and RBS data suggest that the Co particles are highly dispersed and in the pores of the zeolite. Catalytic data suggest that there is a dependence in turnover frequency on the relative size of the particles. Future experiments include the simulation of FMR data at low temperature to determine the dominant anisotropic terms such as particle shape anisotropy, strain ansiotropy, and defect anisotropy.

Acknowledgment. We thank the Office of Basic Energy Sciences, Divisions of Chemical Sciences and Material Sciences (Contract W-31-109-ENG-38), of the Department of Energy for support of this research. We thank Charles Evans and Associates for RBS analyses and Jan Hall of Amoco Chemical Co. for help with the microtoming of samples.

Registry No. Co, 7440-48-4; $CH_3CH{=}CH_2$, 115-07-1; c-C_3H_6, 75-19-4; $CH_3CH_2CH_3$, 74-98-6; CH_4, 74-82-8; CH_3CH_3, 74-84-0.